



Multi-Polarisation C-Band SAR Imagery to Estimate the Recent Dynamics of the d'Iberville Glacier

Mozhgan Zahriban Hesari ^{1,†} , Andrea Buono ^{1,*,†} , Ferdinando Nunziata ^{1,†} , Giuseppe Aulicino ^{2,†}
and Maurizio Migliaccio ^{1,3,†}

¹ Dipartimento di Ingegneria, Università degli Studi di Napoli Parthenope, Centro Direzionale Isola C4, 80143 Naples, Italy

² Dipartimento di Scienze e Tecnologie, Università degli Studi di Napoli Parthenope, Centro Direzionale Isola C4, 80143 Naples, Italy

³ Sezione Osservazione della Terra, Istituto Nazionale di Geofisica e Vulcanologia (INGV), Via di Vigna Murata 605, 00143 Rome, Italy

* Correspondence: andrea.buono@uniparthenope.it

† These authors contributed equally to this work.

Abstract: To monitor polar regions is of paramount importance for climatological studies. Climate change due to anthropogenic activities is inducing global warming that, for example, has resulted in glacier melting. This has had a significant impact on sea levels and ocean circulation. In this study, the temporal trend of the marine-terminated d'Iberville glacier (Ellesmere Island, Canada) is analysed using C-band synthetic aperture radar satellite imagery collected by the Radarsat-2 and Sentinel-1 missions. The data set consists of a time series of 10 synthetic aperture radar data collected from 2010 to 2022 in dual-polarimetric imaging mode, where a horizontally polarised electromagnetic wave was transmitted. An automatic approach based on a global threshold constant false alarm rate method is applied to the single- and dual-polarisation features, namely the HH-polarised normalised radar cross-section and a combination of the HH- and HV-polarised scattering amplitudes, with the aim of extracting the ice front of the glacier and, therefore, estimating its behaviour over time. Independent collocated satellite optical imagery from the Sentinel-2 multi-spectral instrument is also considered, where available, to support the experimental outcomes. The experimental results show that (1) the HH-polarised normalised radar cross-section achieved better performance with respect to the dual-polarised feature, especially under the most challenging case of a sea-ice infested sea surface; (2) when the HH-polarised normalised radar cross-section was considered, the ice front extraction methodology provided a satisfactory accuracy, i.e., a root mean square error spanning from about 1.1 pixels to 3.4 pixels, depending on the sea-surface conditions; and (3) the d'Iberville glacier exhibited, during the study period, a significant retreat whose average surface velocity was 160 m per year, resulting in a net ice area loss of 2.2 km² (0.18 km² per year). These outcomes demonstrate that the d'Iberville glacier is behaving as most of the marine-terminated glaciers in the study area while experiencing a larger ice loss.

Keywords: d'Iberville glacier; C-band SAR; polarisation; Canada; ice front extraction



Citation: Zahriban Hesari, M.; Buono, A.; Nunziata, F.; Aulicino, G.; Migliaccio, M. Multi-Polarisation C-Band SAR Imagery to Estimate the Recent Dynamics of the d'Iberville Glacier. *Remote Sens.* **2022**, *14*, 5758. <https://doi.org/10.3390/rs14225758>

Academic Editor: Andreas J. Dietz

Received: 30 August 2022

Accepted: 9 November 2022

Published: 14 November 2022

Publisher's Note: MDPI stays neutral with regard to jurisdictional claims in published maps and institutional affiliations.



Copyright: © 2022 by the authors. Licensee MDPI, Basel, Switzerland. This article is an open access article distributed under the terms and conditions of the Creative Commons Attribution (CC BY) license (<https://creativecommons.org/licenses/by/4.0/>).

1. Introduction

Global warming has become a critical issue in recent years. According to the latest report of the Intergovernmental Panel on Climate Change, average temperatures between 2001 and 2020 were 0.99 °C higher than those between 1850 and 1900 [1]. Global warming has also had a significant impact on polar regions by significantly reducing the ice masses of glaciers, ice sheets, and ice caps [2].

Glaciers are indeed one of the most important facets of the Earth's ecosystem [3]. Together with icebergs, ice sheets, and the permanent snow cover in the polar regions, glaciers account for 1.7% of the water on Earth [4]. Glaciers are also an important indicator

of climate change since their advancing/retreating dynamics are clear proof of changes in temperature and precipitation [5]. Therefore, monitoring the time evolution of glaciers is a critical issue that can support predictions about how changes in glacier control can affect both the local and global environment [6].

In this context, due to the characteristics of the polar regions, which are mostly inaccessible due to harsh conditions and limited sunlight, microwave satellite remote sensing is an irreplaceable observation tool that provides information on glaciers during both the day and the night, regardless of cloud cover and other adverse weather conditions [7]. One of the most well-established methods for estimating the surface motion of glaciers and ice sheets is interferometric synthetic aperture radar (InSAR), which allows for the measurement of ice movements with very high accuracy [8,9]. The InSAR technique was the basis of some studies that estimated glacier motion in polar regions [9–11]. The main challenges associated with InSAR approaches to monitoring glacier dynamics consist of limited accuracy in the case of fast-moving glaciers or when low coherence applies [12–14]. Together with the estimation of glacier motion using InSAR approaches, SAR imagery is used to extract the ice fronts of glaciers, ice sheets, and ice tongues and to analyse their behaviour over time. This topic was addressed in [15–19], where different methodologies were proposed.

In this study, we analyse the recent dynamics of one of the most important marine-terminating Arctic glaciers, the d’Iberville glacier in Ellesmere Island in the North Canadian state of Nunavut (80.53°N, 77.77°W) (see Figure 1a). This study area represents a challenging scenario compared to the ones traditionally considered for the application of coastline/shoreline extraction methods. The reason is twofold: on one side, the d’Iberville glacier is a marine-terminated glacier, characterised by a particular coastal morphology and orography, i.e., it significantly differs from conventional “open areas” such as coastal harbours, ice tongues, rocky cliffs, and sandy beaches; and on the other side, the sea-surface conditions significantly vary from winter to summer (see the Sentinel-2 true-colour optical images in Figure 1b,c), with the sea surface being completely frozen for most of the year due to the very low temperatures [20]. These issues make the extraction of the glacier’s ice front and its temporal analysis very challenging.

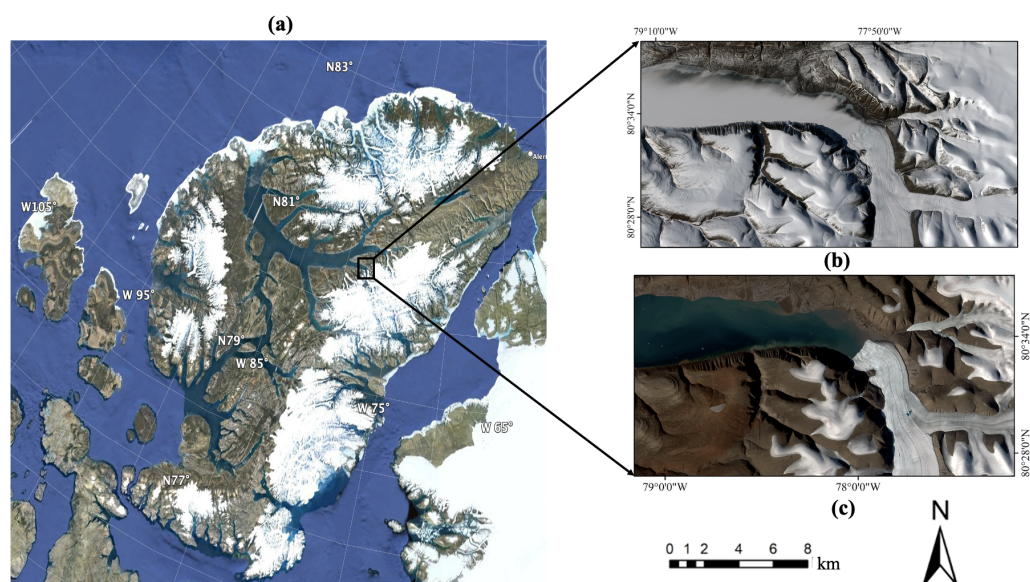


Figure 1. Study area. (a) Google Earth image[®] of the study area that includes Ellesmere Island in the Canadian state of Nunavut. The black square indicates the ice front area of the d’Iberville glacier under investigation. Sentinel-2 true-colour optical images collected over the ice front of the d’Iberville glacier on (b) 26 May 2021 and (c) 26 July 2020.

For this purpose, we apply a methodology to extract the d’Iberville glacier’s ice front from the multi-polarisation C-band SAR imagery, whose backbone relies on a global threshold constant false alarm rate (CFAR) method approach. The latter is applied to the single- and dual-polarisation features, namely the HH-polarised normalised radar cross-section (NRCS) and a combination of the HH- and HV-polarised scattering amplitudes. It must be pointed out that even though the core of this technique has already been applied and validated for different coastal scenarios including the Drygalski ice tongue in Antarctica [18], inland artificial water bodies [21], marshlands/wetlands [22], and rocky cliffs/sandy beaches [23], this is the first time that it is applied and analysed in such a challenging environment. In addition, even though the dynamics of the d’Iberville glacier have already been studied in the past [24–26], there is no updated information on its recent behaviour, i.e., the time evolution of the d’Iberville glacier has been studied up until 2004 and, to the best of our knowledge, the only large-scale glacier information that has been provided in recent years refers to the glaciers of the Northern Hemisphere [2].

The novel contributions of this study with respect to the existing literature can be summarised as follows:

- An analysis of the scattering behaviour of multi-polarisation SAR features and their ability to monitor marine-terminated glaciers.
- An accuracy assessment of the coastline extraction algorithm in a challenging environment characterised by ice-infested seawater.
- The provision of updated quantitative information on the time evolution of the d’Iberville glacier ice front.

The remainder of the paper is organised as follows: the satellite data set collected over the d’Iberville glacier is presented in Section 2, whereas the methodology applied to extract the ice front and analyse its time evolution is described in Section 3; the experimental results are presented in Section 4 and are critically discussed in Section 5; and the conclusions are drawn in Section 6.

2. Satellite Data Set

In this section, the satellite data set used for the purpose of this study is described. C-band SAR data from two satellite missions, namely the Canadian Space Agency Radarsat-2 and the European Space Agency Sentinel-1, were considered. The former is a single SAR satellite mission that was launched in 2007, whereas the latter consists of a constellation of twin SAR satellites that were launched in 2014 and 2016. Three Radarsat-2 SAR scenes were collected over the study area in dual-polarimetric fine imaging mode (HH + HV, i.e., a horizontally polarised electromagnetic wave was transmitted, whereas the backscattered wave was measured on an orthogonal horizontal-vertical polarisation linear basis) from 2010 to 2012 (one scene per year). Seven Sentinel-1 SAR scenes were collected over the study area in dual-polarimetric HH + HV interferometric wide (IW)-swath imaging mode from 2015 to 2022 (one scene per year, except for 2016). The main characteristics of the SAR satellite data set are listed in Table 1.

Table 1. Overview of the satellite SAR data set.

SAR Mission	Number of Scenes	Imaging Mode	Polarisation	Pixel Spacing (m)	Acquisition Period
Radarsat-2	3	Fine dual	HH + HV	6	2010–2012
Sentinel-1	7	IW swath	HH + HV	13	2015–2022

Independent optical data from the European Space Agency Sentinel-2 mission, whose twin satellites were launched in 2015 and 2017 and are equipped with a multi-spectral imager (MSI), were also collected over the d’Iberville glacier. When they were sufficiently cloud-free and time collocated (within ± 3 days) with the SAR scenes, they were used to assess the accuracy performance of the ice front extraction methodology.

3. Methodology

In this section, the methodology adopted to extract the ice front of the d'Iberville glacier and to analyse its dynamics is presented. The methodology has a twofold objective: (1) the extraction of the glacier's ice front, i.e., the boundary between the marine-terminated glacier and the frozen/unfrozen sea surface, from a single SAR image using both the single- and dual-polarisation features; (2) the analysis of the behaviour of the ice front over time to estimate its advancing/retreating velocity and ice area gain/loss. A flowchart of the processing chain is shown in Figure 2, where three main steps can be identified.

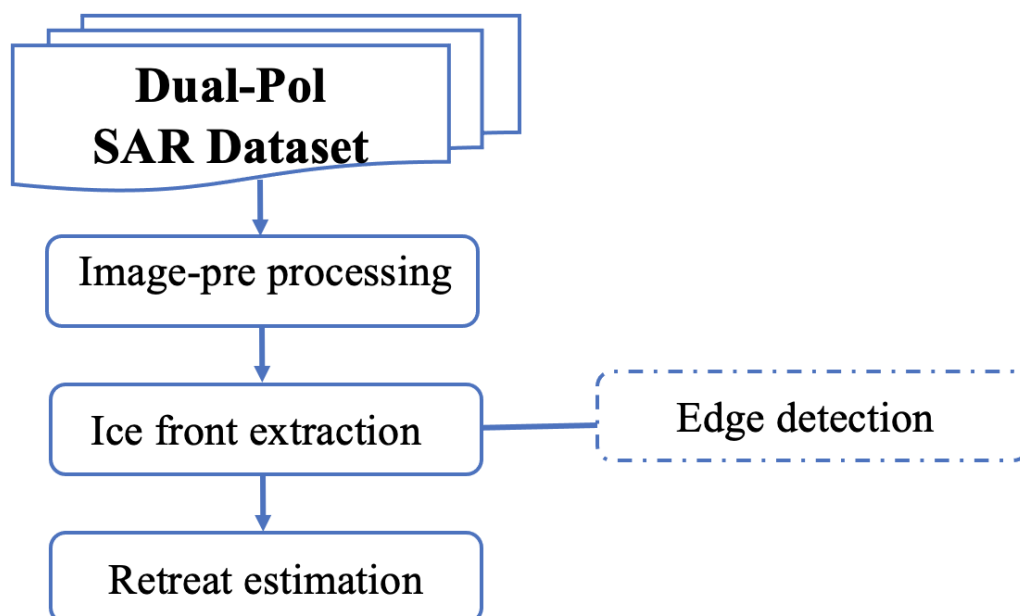


Figure 2. Flowchart of the methodology.

- **Pre-processing step.** All the SAR scenes from the data set were pre-processed using the Sentinel Application Platform (SNAP) v 8.0 software [27] to reduce orbital errors, speckle noise, and geometric distortions. First, radiometric calibration was performed, and then, a 5×5 moving average window was applied to reduce speckle, which could hamper the identification of the ice front. Finally, range-Doppler terrain correction was applied to map the SAR imagery in geographical coordinates, resulting in square pixels with a spacing of 6 m and 13 m for Radarsat-2 and Sentinel-1, respectively (see Table 1).
- **Ice front extraction step.** A CFAR approach was used to distinguish the d'Iberville glacier from the surrounding ice-free or ice-infested sea water, i.e., to extract the ice front. The CFAR method was applied to the HH-polarised NRCS, indicated with σ_{HH}^0 , and to a combination of the HH- and HV-polarised scattering amplitudes, termed ρ [21,22,28]:

$$\sigma_{HH}^0 = \langle |S_{HH}|^2 \rangle \quad (1)$$

$$\rho = \langle |S_{HH}| \cdot |S_{HV}| \rangle \quad (2)$$

where S represents the complex-valued element of the scattering matrix measured by the polarimetric SAR sensor, i.e., the scattering amplitude, with subscripts that refer to the transmitted and received polarisation (H and V mean the horizontal and vertical polarisation, respectively), and the operators $|\cdot|$ and $\langle \cdot \rangle$ stand for the modulus and spatial averaging, respectively. As a result, the CFAR algorithm automatically provides a global threshold for the σ_{HH}^0 and ρ images, thus generating a binary image. A false alarm probability P_{fa} that ranged from 10^{-3} to 10^{-1} was set as the input of the CFAR method, depending on the SAR scene. Once the binary image was obtained, it

was refined by conventional image processing tools, i.e., morphological filters, to sort out clear and isolated false edges at sea. Then, the optimal Canny edge detector, which is based on a two-dimensional Gaussian kernel, was applied to the refined binary image to obtain the actual ice front of the d'Iberville glacier. This processing step was performed using Matlab software version R2021b.

- **Indicators' estimation step.** Once the first two steps were applied to the whole SAR data set, the 10 ice fronts extracted for the d'Iberville glacier were imported into the Aeronautical Reconnaissance Coverage Geographic Information System (ArcGIS) software to quantitatively estimate the surface velocity and extent of the ice gain/loss. The former was obtained by the ratio between the distance measured among the ice fronts extracted from two consecutive SAR scenes and the time between them (in years), whereas the latter was evaluated by estimating the area between the ice fronts extracted from 2010 to 2022.

Further details can be found in [18,21,22,28], where a similar backbone algorithm was used to extract the coastal boundary under different environments.

4. Experimental Results

In this section, the experiments undertaken by applying the methodology described in Section 3 to the data set presented in Section 2 are shown. Three experiments were performed. The first experiment consisted of analysing the sensitivity of the single- and dual-polarisation features (see (1) and (2), respectively) to the different scattering scenarios, i.e., frozen and ice-free sea surfaces (see Figure 3a,d, respectively). The second experiment aimed to investigate the accuracy performance of the ice front extraction of σ_{HH}^0 and ρ under both sea conditions in order to find the feature that achieved the lowest root mean square error (RMSE) between the extracted ice front and the reference one manually extracted from the corresponding Sentinel-2 optical images. The third experiment consisted of analysing the temporal behaviour of the d'Iberville glacier ice front using quantitative indicators such as the ice front surface velocity and the amount of ice surface gain/loss.

For the purpose of the first two experiments, two SAR scenes collected under different sea-surface conditions were selected from the data set according to the shortest time gap between the SAR and MSI acquisitions (see Figure 3). The first one refers to the observation in May 2021 during the winter season when the sea surface was completely frozen due to very low temperatures (see the Sentinel-2 true-colour optical image in Figure 3a). The corresponding σ_{HH}^0 and ρ images are depicted as graytones and false-colour images at the decibel (dB) scale in Figure 3b,c, respectively. The second scene is relevant to the acquisition in July 2020 during the summer season when the sea surface was completely ice-free due to relatively higher temperatures (see the Sentinel-2 true-colour optical image in Figure 3d). The corresponding σ_{HH}^0 and ρ images are shown in Figure 3e,f, respectively.

The first experiment consisted of the analysis of the sensitivity of σ_{HH}^0 and ρ to ice-free and ice-infested sea surfaces. By visually inspecting Figure 3, it can be seen that the separability between the marine-terminating d'Iberville glacier and the frozen sea surface is challenging, even in the Sentinel-2 optical image, making the extraction of the ice front not straightforward. When dealing with the HH-polarised NRCS images, it can be observed that both the frozen and unfrozen sea surfaces appear as almost homogeneous areas that are darker than the terminus of the glacier, which, instead, shows some roughness in the surface pattern. In addition, the difference in backscattering between the sea surface and the glacier appears larger in the unfrozen case than in the case when the sea surface is ice-infested. In fact, in the latter case, the two regions look very similar, except for on the ice front, which appears as a brighter edge. When dealing with the ρ images, similar comments apply.

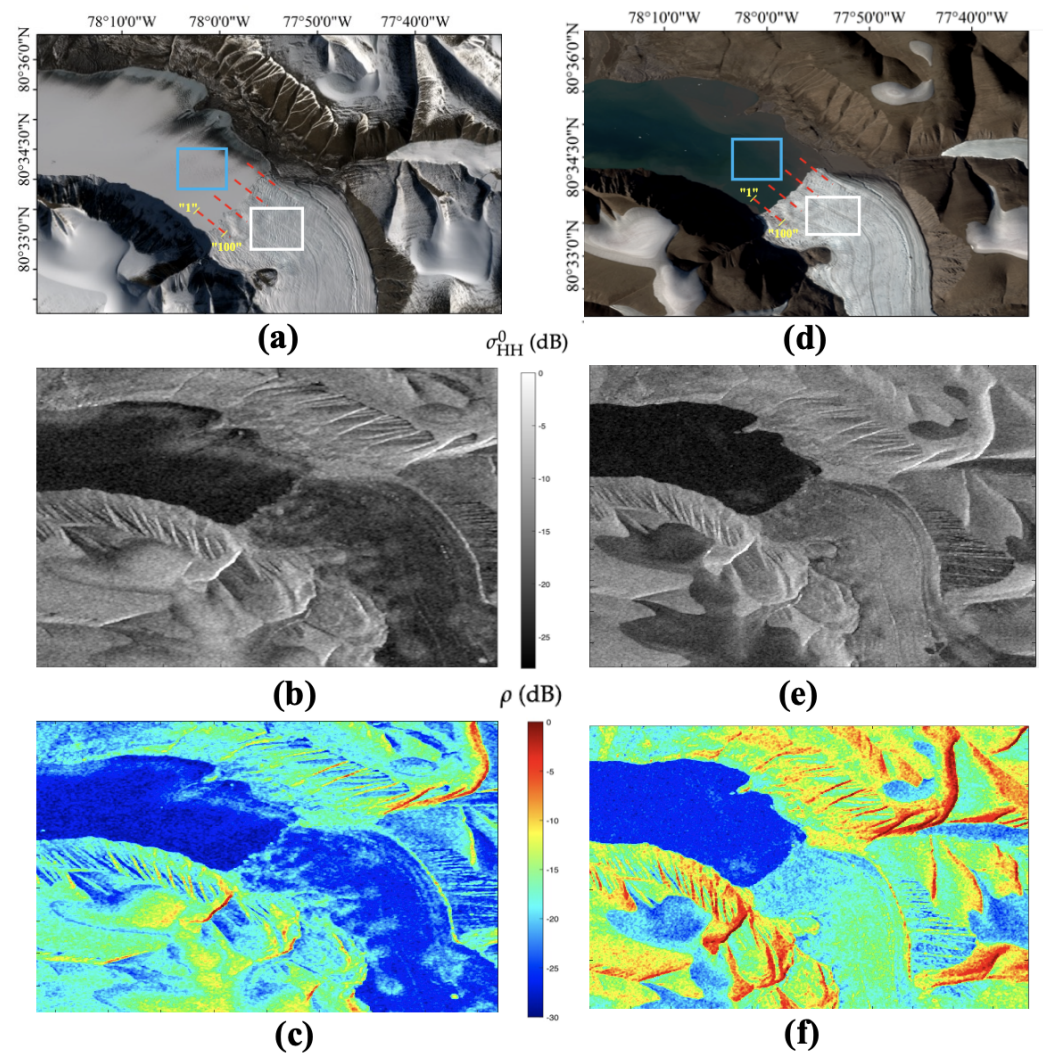


Figure 3. Selected scenes relevant to frozen (a–c) and ice-free (d–f) sea surfaces. Panels (a,d) show the reference Sentinel-2 MSI true-colour optical images; (b,e) show the graytone σ_{HH}^0 images at the dB scale; (c,f) show the false-colour ρ images depicted at the dB scale. In panels (a,d), cyan and white squares indicate the sea and glacier ROIs, respectively, which are randomly excerpted for quantitative scattering analysis (see Table 2). The four transects randomly selected for quantitative scattering analysis are also indicated by red dashed lines, where the first and last pixels of the transect are labelled “1” and “100”, respectively, and marked in yellow.

Table 2. Mean and standard deviation values of the considered features evaluated for the selected ROIs shown in Figure 3a,d.

SAR Feature	Case	Sea ROI (Mean \pm Std in dB)	Glacier ROI (Mean \pm Std in dB)	Mean Contrast (dB)
σ_{HH}^0	Unfrozen	-23.8 ± 1.0	-15.7 ± 1.1	8.1
ρ	Unfrozen	-26.3 ± 0.7	-21.8 ± 0.9	4.5
σ_{HH}^0	Frozen	-22.0 ± 1.0	-15.9 ± 1.3	6.1
ρ	Frozen	-25.2 ± 0.8	-20.4 ± 1.1	4.8

To perform a quantitative multi-polarisation backscattering analysis, two equal-sized regions of interest (ROIs) consisting of 100×100 pixels were randomly selected from the sea and glacier areas close to the ice front (see the cyan and white squares, respectively, which are annotated in Figure 3a,b). The statistical behaviours estimated for σ_{HH}^0 and ρ for

the selected ROIs under both frozen and unfrozen sea conditions are shown in Figure 4, where experimental histograms are depicted using blue (sea ROI) and orange (glacier ROI). In Figure 4, the rows refer to the unfrozen and frozen cases, whereas the columns refer to σ_{HH}^0 and ρ . The corresponding mean and standard deviation values of σ_{HH}^0 and ρ are listed in Table 2. The mean contrast is also annotated as a rough indicator of the separability between the sea and glacier ROIs in terms of multi-polarisation backscattering.

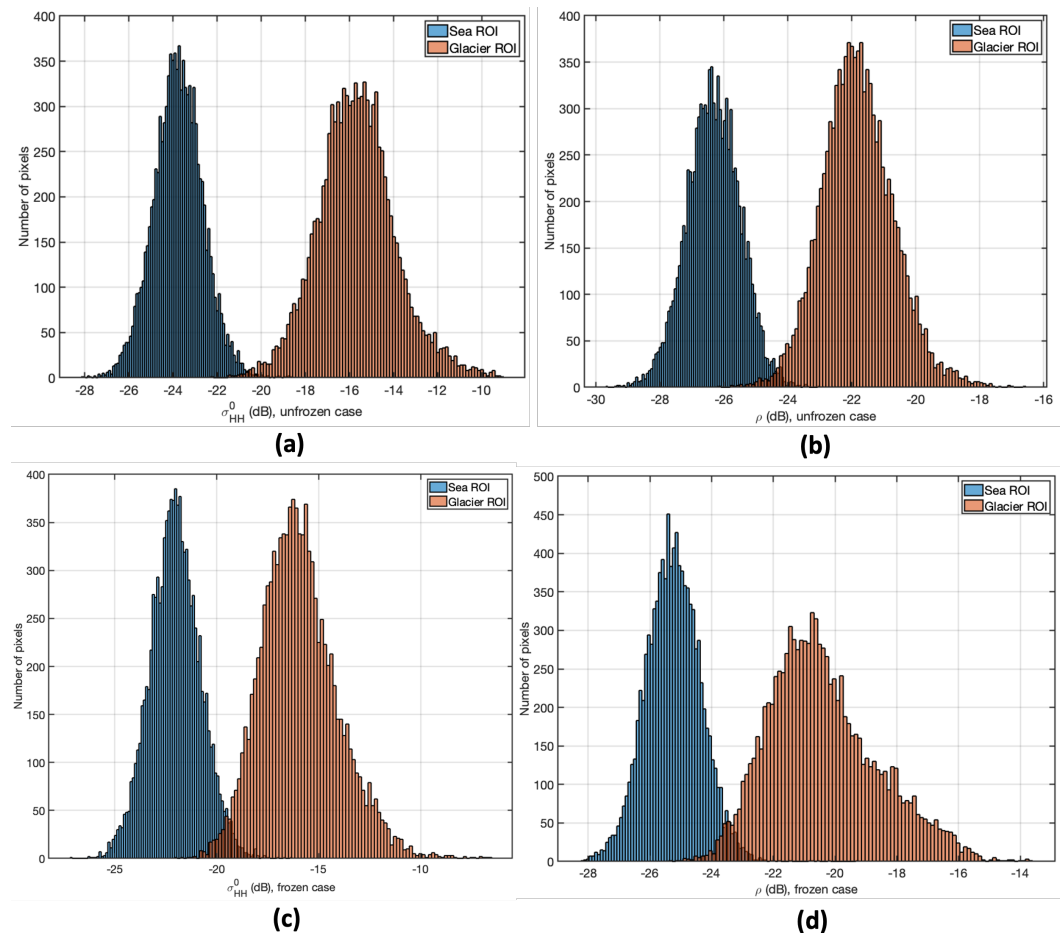


Figure 4. Statistical behaviours of single- and dual-polarimetric features evaluated for the 10^4 samples belonging to the selected ice-free and ice-infested seas (in blue) and glacier (in orange) ROIs. Rows refer to histograms estimated for the unfrozen (a,b) and frozen cases (c,d), respectively, whereas columns refer to histograms obtained from σ_{HH}^0 (a,c) and ρ (b,d), respectively. The corresponding mean and standard deviation values are listed in Table 2.

When dealing with the unfrozen case, for the seawater ROI, σ_{HH}^0 and ρ had average values of about -24 dB and -26.5 dB, whereas they increased to approximately -15.5 dB and -22 dB, respectively, for the glacier ROI. This resulted in a mean contrast, which was no lower than 4.5 dB on average for both features. Nonetheless, it is worth noting that the mean contrast between the seawater and glacier ROIs provided by σ_{HH}^0 , i.e., 8.1 dB, was more than 3.5 dB higher than the one evaluated from ρ (4.5 dB).

When dealing with the frozen case, σ_{HH}^0 and ρ were characterised by average sea (glacier) ROI values of about -22 dB and -25 dB (-16 dB and -20.5 dB). This resulted in a mean contrast of 6.1 dB and 4.8 dB for σ_{HH}^0 and ρ , respectively, proving that even in this case, the HH-polarised NRCS provided a higher glacier/ice-infested seawater separability.

A deeper analysis was undertaken by evaluating the behaviour of σ_{HH}^0 and ρ along four randomly selected transects crossing the sea/glacier boundary. They are annotated as red dashed lines in Figure 3a,d. The transects consisted of 100 pixels each, where

pixels “1” and “100” refer to the transect’s sea and glacier pixels farthest from the ice front, respectively (see yellow labels in Figure 3a,d), whereas the latter was at pixel number “50”. The results relevant to the ice-free and ice-covered sea surfaces are shown in Figures 5 and 6, respectively, where black and blue dashed lines refer to the σ_{HH}^0 and ρ values obtained after averaging along the four transects, respectively. In addition, for reference purposes, the mean values evaluated for the sea and glacier ROIs are shown in Figure 3a,d and Table 2, and they are annotated using the same colour coding but with continuous lines.

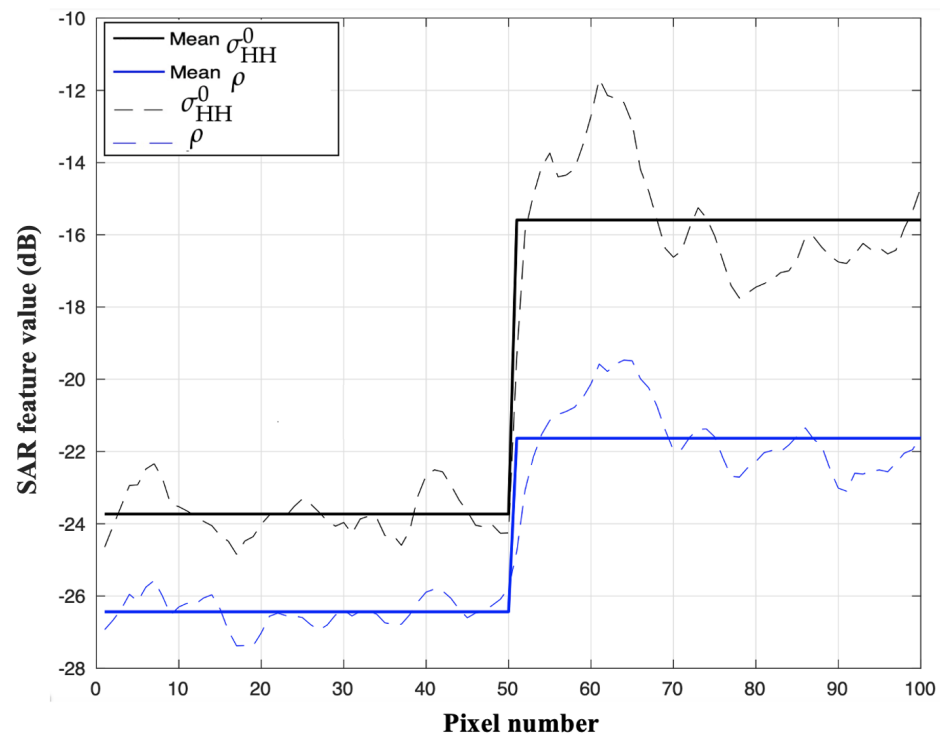


Figure 5. Unfrozen case. Dashed lines refer to σ_{HH}^0 (black) and ρ (blue) values evaluated as an average over the four transects shown with red dashed lines in Figure 3a,d. For reference purposes, the σ_{HH}^0 (black) and ρ (blue) mean values estimated for the sea and glacier ROIs (see Table 2 and Figure 3a,d) are depicted as continuous lines.

When dealing with the unfrozen case, it can be observed that the σ_{HH}^0 values were in the range of about -25 to -22 dB for the ice-free sea surface, whereas for the glacier, they increased to approximately -18 to -12 dB (see Figure 5). Considering the dual-polarisation feature, i.e., ρ , values from about -27 to -26 dB were observed for the unfrozen sea, whereas they increased to a range of approximately -23 to -19 dB for the glacier.

Considering the frozen case, different comments apply (see Figure 6). In fact, even though the glacier area was closer to the ice front (pixel number “50”), the σ_{HH}^0 and ρ values were almost the same as those observed for the unfrozen case; the freezing of the sea surface resulted in a different multi-polarisation backscattering that yielded slightly higher values (about $+2$ dB) for both the single- and dual-polarisation features.

The second experiment consisted of evaluating the accuracy of the methodology used for extracting the d’Iberville glacier ice front. The performance of the σ_{HH}^0 and ρ features were analysed under both frozen and unfrozen sea conditions. The quantitative assessment was based on the RMSE values estimated between the ice front extracted from the SAR imagery and the ice front manually traced from the corresponding reference Sentinel-2 true-colour optical images.

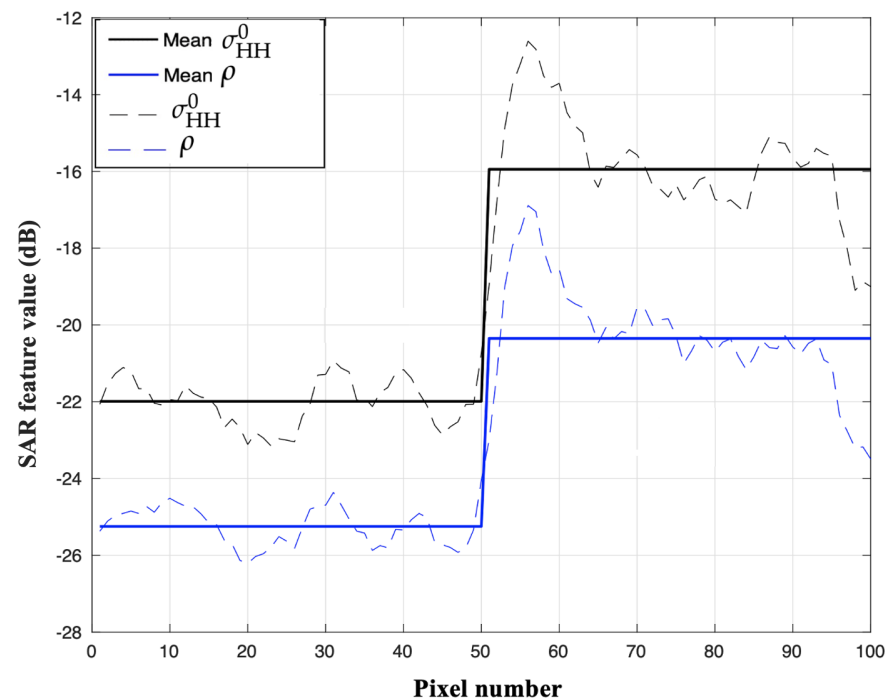


Figure 6. Frozen case. Dashed lines refer to σ_{HH}^0 (black) and ρ (blue) values evaluated as an average over the four transects shown with red dashed lines in Figure 3a,d. For reference purposes, the σ_{HH}^0 (black) and ρ (blue) mean values estimated for the sea and glacier ROIs (see Table 2 and Figure 3a,d) are depicted as continuous lines.

The results relevant to the unfrozen case are shown in Figure 7, where the ice fronts extracted from σ_{HH}^0 and ρ , which are depicted in red and green, respectively, are overlapped on the reference optical image. An inset is also shown to better appreciate the results (see the yellow box). It can be seen that the ice fronts extracted from both features resulted in a good visual agreement with the actual ice front profile obtained from the optical image, even though some non-negligible false alarms occurred along the north-eastern edge of the d'Iberville glacier ice front. A visual inspection also suggests that σ_{HH}^0 resulted in a slightly better accuracy with respect to ρ , as already inferred from the outcomes of the first experiment. To perform a quantitative analysis, 20 points were randomly selected along the ice fronts and the RMSE was evaluated between the peer points belonging to the ice fronts extracted from the SAR image (σ_{HH}^0 and ρ) and the ones manually traced from the corresponding Sentinel-2 optical image. We found that σ_{HH}^0 had an RMSE of 1.18 pixels, whereas ρ had an RMSE of 2.97 pixels. The same analysis was performed for the frozen case (see Figure 8). As expected, due to the more challenging scattering conditions, larger RMSE values were obtained, i.e., 3.35 pixels for σ_{HH}^0 and 4.56 pixels for ρ .

The third experiment consisted of investigating the temporal behaviour of the d'Iberville glacier ice front from 2010 to 2022. On the basis of the results of the previous experiments, the ice front was extracted from the HH-polarised NRCS images of the whole SAR data set. The results are shown in Figure 9, where the study area is masked in white, except for the 10 ice fronts extracted from σ_{HH}^0 , which are depicted using different colours. Figure 9 clearly shows that the d'Iberville glacier exhibited a net retreat over the last 12 years (see the red and yellow ice fronts that refer to 2010 and 2022, respectively). To quantitatively analyse the retreating rate of the d'Iberville glacier, the average surface velocity was estimated by measuring, for each couple of consecutive years in the SAR data set, the distance between the two ice fronts computed from the same points randomly selected for the evaluation of the RMSE divided by the number of years. The average surface velocity estimated in such a way is listed in Table 3. It can be seen that the retreating rate of the d'Iberville glacier varied significantly over time. In fact, the very fast retreat during 2010–2011, when the

d'Iberville glacier had an average surface velocity of 514 m/year, corresponds to the almost stable behaviour of the d'Iberville glacier during 2021–2022, when it was characterised by an average surface velocity of 28 m/year. However, on average, from 2010 to 2022 the d'Iberville glacier retreated with an average surface velocity of 160 m per year. Together with the average surface velocity, the net ice loss from the glacier's surface was estimated by measuring the area between the ice fronts extracted in 2010 and 2022 (see Figure 10), where the extent of the retreat is highlighted in cyan. The latter corresponds to an ice area of about 2.2 km², meaning that, on average, the d'Iberville glacier experienced an ice loss of about 0.18 km² per year from 2010 to 2022.

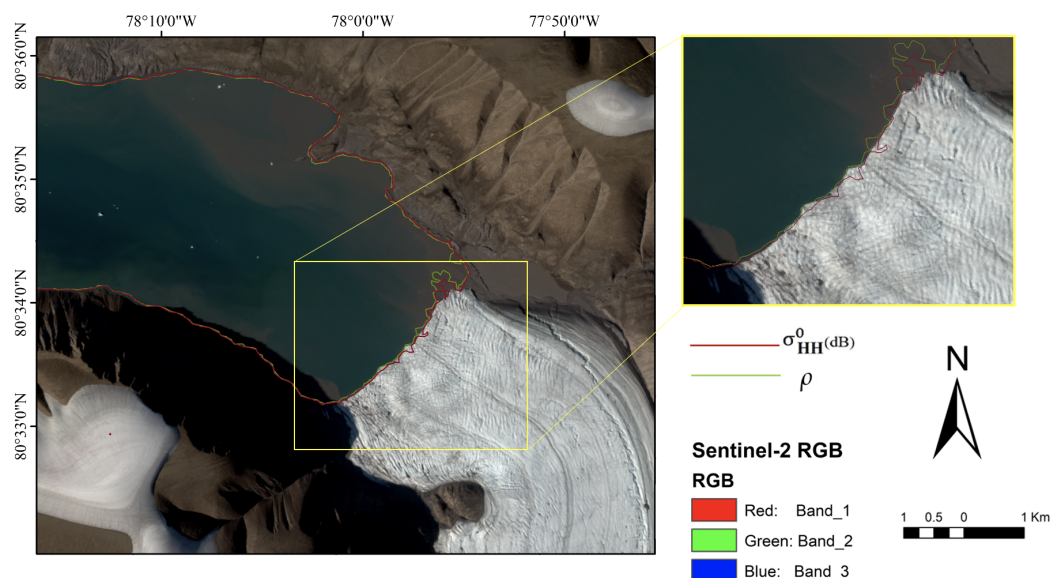


Figure 7. Accuracy assessment of the ice front extraction in the unfrozen case. Ice fronts extracted from σ_{HH}^0 (red) and ρ (green) are overlaid on the reference optical (Red-Green-Blue, RGB) image collected by the Sentinel-2 MSI on 26 July 2020. An enlarged version, highlighted by the yellow box, is shown to better appreciate the results.

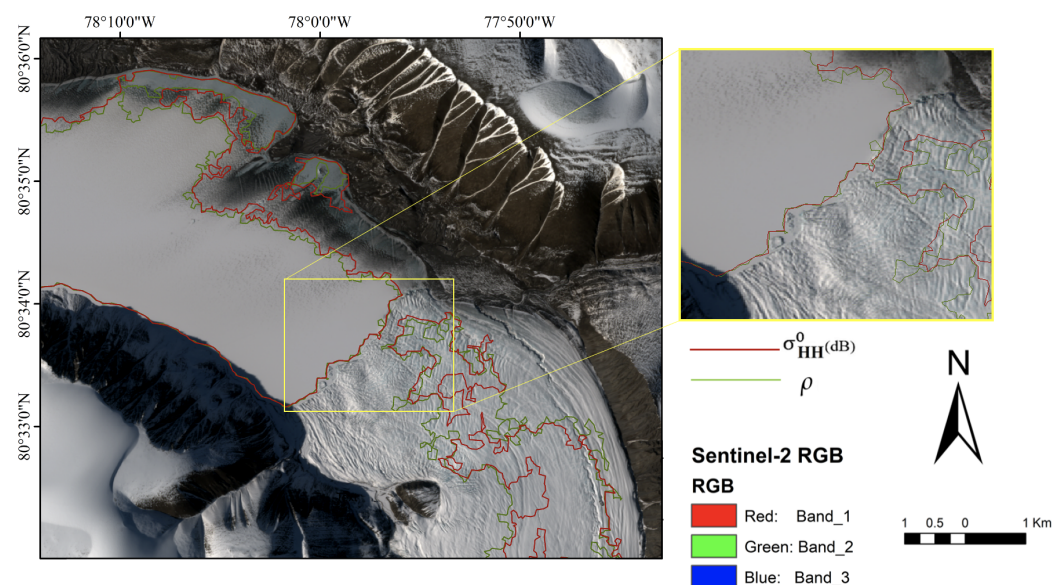


Figure 8. Accuracy assessment of the ice front extraction in the unfrozen case. Ice fronts extracted from σ_{HH}^0 (red) and ρ (green) are overlaid on the reference optical (RGB) image collected by the Sentinel-2 MSI on 26 May 2021. An enlarged version, highlighted by the yellow box, is shown to better appreciate the results.

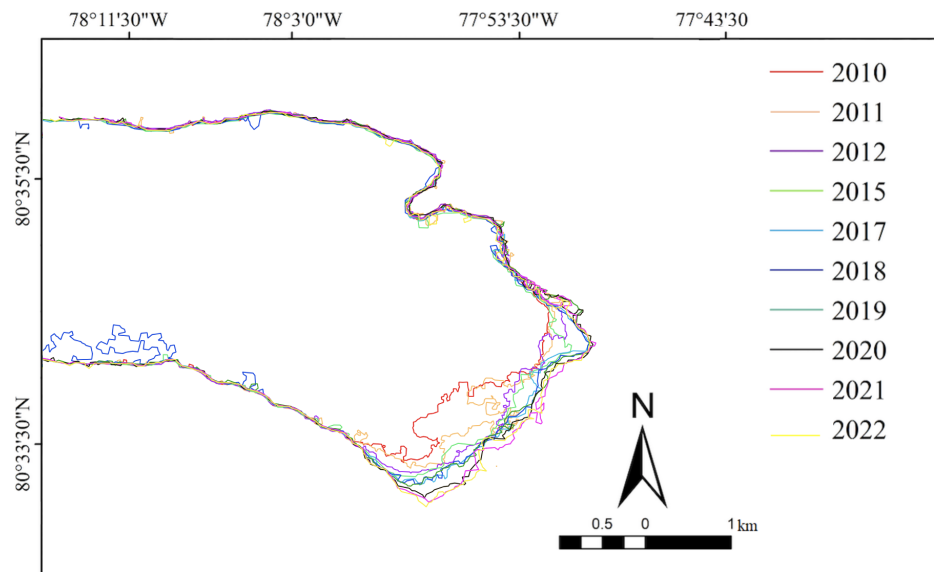


Figure 9. Ice fronts of the d'Iberville glacier extracted from the HH-polarised NRCS from 2010 to 2022.

Table 3. Average retreating surface velocities of the d'Iberville glacier ice front estimated from the experimental results shown in Figure 9.

Year	Surface Velocity (m per Year)
2010–2011	514
2011–2012	326
2012–2015	81
2015–2017	90
2017–2018	108
2018–2019	136
2019–2020	196
2020–2021	142
2021–2022	28

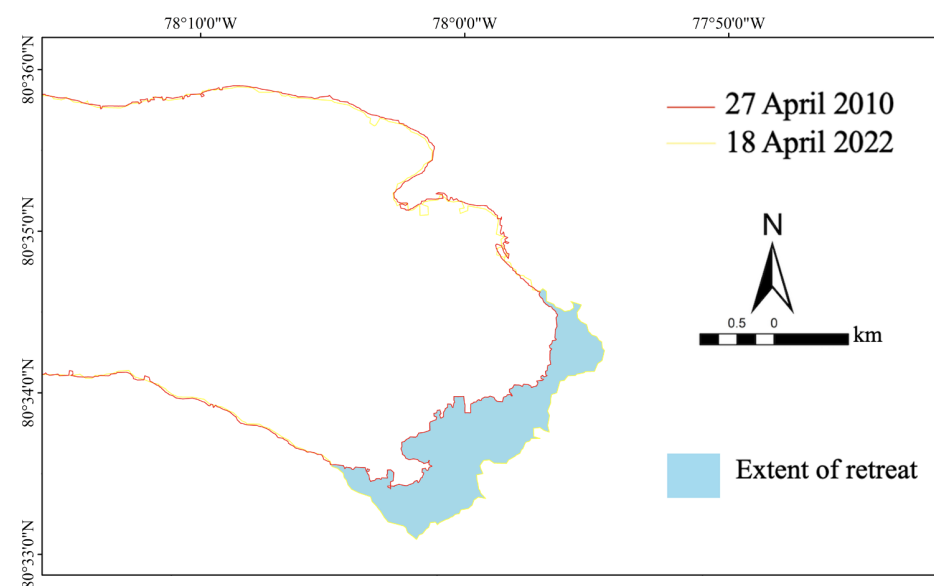


Figure 10. Estimation of the d'Iberville glacier retreat extent obtained from the ice fronts extracted in 2010 and 2022 from σ_{HH}^0 .

5. Discussion

In this section, the experimental results presented in Section 4 are critically discussed. First, the results of the first two experiments are discussed to analyse the characteristics and the potential of the method used for the ice front extraction. Then, the outcomes of the third experiment are discussed against state-of-the-art studies that provided information on the time variability of the d'Iberville glacier using remote sensing tools. The latter are first presented with respect to the average surface velocity of the d'Iberville glacier and, then, the behaviour of the d'Iberville glacier over time is contrasted on a larger scale by comparing it with the temporal trends exhibited by other marine-terminated glaciers in the same area, i.e., Ellesmere Island and the whole North Canadian Arctic. Nonetheless, it must be pointed out that very few studies have addressed the temporal trend of the d'Iberville glacier's morphological features and none of them covers the same analysis period investigated in this study.

The first experiment dealt with a sensitivity analysis of the ice front extraction to multi-polarisation backscattering features and sea-surface conditions. Accordingly, the behaviour of the single- and dual-polarisation parameters, i.e., σ_{HH}^0 and ρ , was investigated for ice-free and ice-infested seawater to gain deeper insights into the ice front extraction capabilities. The experimental results are shown in Figures 3–6 and listed in Table 2.

With respect to the sea-state conditions, the results suggest that both the single- and dual-polarisation features provided a remarkable mean contrast, i.e., ≥ 4.5 dB, for both the frozen and unfrozen cases, proving that they allow for a robust and accurate ice front extraction. However, the results also suggest that the extraction of the ice front was more challenging when the sea surface was frozen, independent of the considered SAR feature. In fact, the presence of sea ice resulted in a larger multi-polarisation backscattering at sea. As a result, when moving from the ice-free to the sea-ice-infested case, the mean contrast reduced by about 25% when dealing with σ_{HH}^0 and remained almost stable, i.e., it increased by less than 7% when ρ was considered. This makes the ice front extraction of the d'Iberville glacier using satellite imagery a challenging task since there are likely to be frozen sea-surface conditions in the study area. In fact, according to the average temperature records obtained for the Nunavut area for the last 30 years, the minimum temperature is below the seawater freezing point for 9 months each year [20]. Hence, the sea-ice-infested seawater case can be considered the most frequent case when extracting the d'Iberville glacier ice front.

With respect to the SAR feature, the results suggest that the HH-polarised NRCS provided, on average, a larger scattering separability compared to ρ , regardless of the sea-state conditions. In fact, the mean contrasts estimated for σ_{HH}^0 were 80% and 27% higher than those of ρ under ice-free and ice-infested conditions, respectively. Hence, since ρ was constructed by adding the cross-polarised information (HV channel) to the co-polarised information (HH channel) (see (2)), by moving from the single- to the dual-polarisation feature, the cross-polarised information contributed to the sea and glacier ρ values being closer than those in the case of σ_{HH}^0 . In fact, even though for the sea surface, ρ values lower than about 2.5–3 dB with respect to σ_{HH}^0 ones were advisable, this was no longer the case for the glacier's surface, where the ρ values were significantly lower, i.e., about 4.5–6 dB, compared to those of the corresponding σ_{HH}^0 . This proves that including the cross-polarised information according to (2) does not allow for a larger contrast under any sea-state conditions, as found in [21,22,28] but for different coastal scenarios such as sandy beaches, cliffs, and marshlands. Hence, worse ice front extraction performance was expected when ρ was considered.

The second experiment dealt with an accuracy assessment of the ice front extraction performance. Accordingly, the ice front of the d'Iberville glacier was extracted from both the single- and dual-polarisation parameters, i.e., σ_{HH}^0 and ρ , and, then, the RMSE was evaluated with respect to the reference ice fronts manually traced from the corresponding Sentinel-2 optical images. The experimental results are shown in Figures 7 and 8, which refer to the unfrozen and frozen cases, respectively. They confirmed that (1) the methodology

used in this study to extract the ice front of the d'Iberville glacier was effective and accurate regardless of the sea-state conditions and SAR features since an RMSE lower than 5 pixels was obtained in any case; (2) the ice front extraction was more challenging during the winter season, i.e., when the sea surface was frozen since the RMSE increased by approximately 184% and 54% for σ_{HH}^0 and ρ , respectively; and (3) σ_{HH}^0 resulted in a better extraction accuracy compared to ρ since RMSEs lower than about 60% and 27% were achieved under unfrozen and frozen sea-state conditions, respectively. The accuracies reported in Section 4 represent fairly good results compared with similar approaches presented in the literature to extract the coastline from C-band SAR imagery using multi-polarisation features. In fact, mean distances of 4.6 pixels and 5.4 pixels were achieved in the extraction of the coastal profile from ρ for a sandy beach and a marshland/mudflat area in [22,28], respectively, whereas an RMSE of 2.3 pixels was obtained in [18] when extracting the ice front of an ice tongue from σ_{HH}^0 under ice-free sea conditions.

The third experiment dealt with a time-variability analysis of the ice front. To this aim, two quantitative indicators were provided, i.e., the average surface velocity and the average ice area variation. The experimental results are shown in Table 3 and Figures 9 and 10.

In this study, we estimated that the d'Iberville glacier was retreating with an average surface velocity of about 160 m per year in the period 2010–2022. We found that the retreat velocity significantly changed over time and that the most remarkable and fastest retreat was observed between 2010 and 2011 (see red and orange ice fronts in Figure 9, respectively). This behaviour is compatible with recent global warming, which is becoming increasingly more intense than that in the past [29]. In fact, temperature records relevant to the Nunavut area provided an average annual temperature for 2010 of -10.7 °C, i.e., 2.5 °C higher than the mean temperature measured for the period 2010–2021.

The retreat of the d'Iberville glacier was also observed in [24] where a significantly much larger surface velocity, i.e., about 480 m per year, was estimated. Nonetheless, it should be pointed out that the results were obtained from aerial photographs and for the year 1975 only. A lower surface velocity, i.e., 300 m/year, was estimated using a C-band SAR for the year 1991 [30]. The average surface velocity in a more recent period, i.e., from 1999 to 2004, was estimated using optical and C-band SAR satellite instruments, respectively, in [25,26]. Their outcomes matched quite well with our results since they found that the ice front of the d'Iberville glacier retreated with a surface velocity ranging from 30 m (1999–2003) to 105 m (2003–2004) per year. A longer and more recent period, i.e., 1999–2015, was investigated using optical and C-band SAR satellite imagery in [29] where, even though the surface velocity was not explicitly estimated, they found that the d'Iberville glacier experienced an average ice mass discharge of 0.01 Gt per year over that period.

When comparing the behaviour of the d'Iberville glacier with other marine-terminated glaciers in the Northern Hemisphere, reference is made to [2,29], where a comprehensive analysis was provided for 16 glaciers in Ellesmere Island over the period 1999–2015 and for 252 glaciers in the North Canadian Arctic over the period 2000–2020. The retreating trend with an average surface velocity of 160 m per year that we estimated for the d'Iberville glacier in the period 2010–2022 is compatible with the large majority, i.e., 75%, of the glaciers in Ellesmere Island, for which an average ice front retreat of about 150 m per year was observed [29].

The average ice surface loss rate we found for the d'Iberville glacier, i.e., 0.18 km² per year, agrees quite well with the findings presented in [2] for the marine-terminated glaciers in the North Canadian Arctic. In fact, an almost constant net ice area loss of 0.12 km² per year was found on average for the 252 glaciers under analysis. This means that the d'Iberville glacier is experiencing an ice area loss that is 50% higher than those of the other North Canadian Arctic marine-terminated glaciers. By restricting this analysis to the overlapping period, i.e., 2010–2020, the average ice area loss rate of the d'Iberville glacier is about 54% higher than that of the one characterising the other marine-terminated glaciers in the North Canadian Arctic.

6. Conclusions

In this study, the recent time evolution of the marine-terminated d'Iberville glacier (Ellesmere Island, Canada) is addressed. To this aim, a time series of 10 dual-polarimetric HH + HV C-band SAR imagery collected by Radarsat-2 and Sentinel-1 satellite missions from 2010 to 2022 is exploited.

First, an unsupervised methodology based on the combination of a global threshold CFAR approach and Canny edge detection is applied for the first time in such a challenging scenario to extract the ice front of the d'Iberville glacier. Single- and dual-polarisation features, namely the HH-polarised NRCS (σ_{HH}^0) and a combination of the HH- and HV-polarised scattering amplitudes (ρ), and two scattering scenarios, i.e., frozen and unfrozen sea surfaces, are considered for the analysis. Then, the accuracy of this methodology is assessed according to the RMSE metric by comparing the ice fronts extracted from the SAR images with the corresponding ice fronts manually traced from the independent cloud-free Sentinel-2 optical images timely collocated with the SAR scenes. Once the validation is performed, the dynamics of the d'Iberville glacier during the study period are quantified by evaluating, from the extracted ice fronts, the annual average surface velocity and the net ice area loss.

The experimental results show that the HH-polarised NRCS provides more reliable and accurate results in extracting the ice front in both the ice-free and ice-infested sea-surface cases. With respect to the reference ice front manually extracted from the Sentinel-2 optical images, the ice front automatically extracted from σ_{HH}^0 has an RMSE lower than 3.4 pixels, regardless of the sea-state conditions. The results also demonstrate that since 2010, the d'Iberville glacier has been experiencing a remarkable retreat with an average surface velocity of 160 m/year, with the most significant retreat observed from 2010 to 2011 due to the very warm local temperatures recorded for 2010. Overall, a net ice loss of 2.2 km², i.e., about 0.18 km² per year, is estimated for the last 12 years. These outcomes show that the d'Iberville glacier is retreating as with most of the marine-terminated glaciers in the study area, though with a larger ice loss.

Author Contributions: Conceptualization, A.B., F.N. and M.M.; methodology, A.B. and F.N.; software, M.Z.H.; validation, M.Z.H. and G.A.; formal analysis, M.Z.H., A.B. and G.A.; data curation, A.B. and M.Z.H.; writing—original draft preparation, M.Z.H.; writing—review and editing, A.B., F.N. and M.M.; supervision, G.A. and M.M.; project administration, F.N. and M.M. All authors have read and agreed to the published version of the manuscript.

Funding: This research was partly funded by the Italian National Programme for Research in Antarctica under the project “Sea-ice—Wave Interaction Monitoring for Marginal Ice Navigation (SWIMMING)”, grant PNRA18_00298.

Data Availability Statement: Not applicable.

Acknowledgments: The authors would like to thank the European Space Agency for providing the free-of-charge Sentinel-1 SAR data through the Copernicus Scientific Open Hub and the Radarsat-2 SAR data under the framework of the Dragon 5 cooperation project ID 57979 “Monitoring harsh Coastal environments and Ocean Surveillance using radar remote sensing sensors”.

Conflicts of Interest: The authors declare no conflict of interest.

Abbreviations

The following abbreviations are used in this manuscript:

ArcGIS Aeronautical reconnaissance coverage Geographic Information System
CFAR Constant False Alarm Rate

dB	decibel
HH	Horizontal transmit Horizontal receive
HV	Horizontal transmit Vertical receive
InSAR	INterferometric SAR
IW	interferometric wide
MSI	multispectral imager
NRCS	normalised radar cross-section
RGB	Red Green Blue
RMSE	root mean square error
ROI	region of interest
SAR	Synthetic Aperture Radar
SNAP	SeNtinel Application Platform
std	standard deviation

References

1. Masson-Delmotte, V.; Zhai, P.; Pirani, A.; Connors, S.L.; Péan, C.; Berger, S.; Caud, N.; Chen, Y.; Goldfarb, L.; Gomis, M.I. Contribution of working group I to the sixth assessment report of the intergovernmental panel on climate change. *Clim. Chang.* **2021**, *epub ahead of print*.
2. Kochtitzky, W.; Copl, L. Retreat of northern hemisphere marine-terminating glaciers, 2000–2020. *Geophys. Res. Lett.* **2022**, *49*, e2021GL096501. [[CrossRef](#)]
3. United States Geological Survey. Available online: <https://www.usgs.gov/special-topics/water-science-school/science/ice-snow-and-glaciers-and-water-cycle> (accessed on 29 July 2022).
4. Oceanwide Expeditions. Available online: <https://oceanwide-expeditions.com/blog/majestic-glaciers-and-icebergs-of-the-arctic-and-antarctica> (accessed on 21 July 2022).
5. Haeberli, W.; Cihlar, J.; Barry, R.G. Glacier monitoring within the global climate observing system. *Ann. Glaciol.* **2000**, *31*, 241–246. [[CrossRef](#)]
6. Karpilo, R.D. Glacier monitoring techniques. In *Geological Monitoring*; Young, R., Norby, L., Eds.; Geological Society of America: Boulder, CO, USA, 2009; pp. 141–162.
7. Raup, B.H.; Andreassen, L.; Bolch, T. Remote sensing of glaciers. In *Remote Sensing of the Cryosphere*; Tedesco, M., Ed.; Wiley: Hoboken, NJ, USA, 2014; pp. 123–156.
8. Rott, H. Advances in interferometric synthetic aperture radar (InSAR) in earth system science. *Prog. Phys. Geogr.* **2009**, *33*, 769–791. [[CrossRef](#)]
9. Gray, L. Using multiple RADARSAT InSAR pairs to estimate a full three-dimensional solution for glacial ice movement. *Geophys. Res. Lett.* **2011**, *38*. [[CrossRef](#)]
10. Rignot, E.; Mouginot, J.; Scheuchl, B. *Measures InSAR-Based Antarctica Ice Velocity Map*; Version 1; NASA National Snow and Ice Data Center Distributed Active Archive Center: Boulder, CO, USA, 2011.
11. Nagler, T.; Wuite, J.; Libert, L.; Hetzenecker, M.; Keuris, L.; Rott, H. Continuous monitoring of ice motion and discharge of Antarctic and Greenland ice sheets and outlet glaciers by Sentinel-1 A & B. In Proceedings of the IEEE International Geoscience and Remote Sensing Symposium IGARSS, Brussels, Belgium, 11–16 July 2021; pp. 1061–1064.
12. Mouginot, J.; Scheuchl, B.; Rignot, E. Mapping of ice motion in Antarctica using synthetic-aperture radar data. *Remote Sens.* **2012**, *4*, 2753–2767. [[CrossRef](#)]
13. Sánchez-Gámez, P.; Navarro, F.J. Glacier surface velocity retrieval using D-InSAR and offset tracking techniques applied to ascending and descending passes of Sentinel-1 data for southern Ellesmere ice caps, Canadian Arctic. *Remote Sens.* **2017**, *9*, 442. [[CrossRef](#)]
14. Hoen, E.W.; Zebker, H.A. Penetration depths inferred from interferometric volume decorrelation observed over the Greenland ice sheet. *IEEE Trans. Geosci. Remote Sens.* **2021**, *38*, 2571–2583.
15. Paravididakis, V.; Ragia, L.; Moirogiorgou, K.; Zervakis, M.E. Automatic coastline extraction using edge detection and optimization procedures. *Geosciences* **2018**, *8*, 407. [[CrossRef](#)]
16. Yu, Y.; Zhang, Z.; Shokr, M.; Hui, F.; Cheng, X.; Chi, Z.; Heil, P.; Chen, Z. Automatically extracted Antarctic coastline using remotely-sensed data: An update. *Remote Sens.* **2019**, *11*, 1844. [[CrossRef](#)]
17. Baumhoer, C.A.; Dietz, A.J.; Kneisel, C.; Kuenzer, C. Automated extraction of Antarctic glacier and ice shelf fronts from Sentinel-1 imagery using deep learning. *Remote Sens.* **2019**, *11*, 2529. [[CrossRef](#)]
18. Zahriban Hesari, M.; Nunziata, F.; Aulicino, G.; Buono, A.; Migliaccio, M. Analysis of fine-scale dynamics of the Drygalski ice tongue in Antarctica using satellite SAR data. *Int. J. Remote Sens.* **2022**, *43*, 2602–2619. [[CrossRef](#)]
19. Pandit, P.; Jawak, S.; Luis, A. Estimation of velocity of the polar record glacier, Antarctica using Synthetic Aperture Radar (SAR). *Proceedings* **2018**, *2*, 332.
20. Climate Change Knowledge Portal. Available online: <https://climateknowledgeportal.worldbank.org/country/greenland/climate-data-historical> (accessed on 29 August 2022).

21. Ferrentino, E.; Nunziata, F.; Buono, A.; Urciuoli, A.; Migliaccio, M. Multipolarization time series of Sentinel-1 SAR imagery to analyze variations of reservoirs' water body. *IEEE J. Sel. Top. Appl. Earth Obs. Remote Sens.* **2020**, *13*, 840–846.
22. Ferrentino, E.; Buono, A.; Nunziata, F.; Marino, A.; Migliaccio, M. On the use of multipolarization satellite SAR data for coastline extraction in harsh coastal environments: The case of Solway Firth. *IEEE J. Sel. Top. Appl. Earth Obs. Remote Sens.* **2020**, *14*, 249–257. [[CrossRef](#)]
23. Buono, A.; Nunziata, F.; Mascolo, L.; Migliaccio, M. A Multipolarization analysis of coastline extraction using X-band COSMO-SkyMed SAR data. *IEEE J. Sel. Top. Appl. Earth Obs. Remote Sens.* **2014**, *7*, 2811–2820. [[CrossRef](#)]
24. Holdsworth. Ice flow and related measurements of d'Iberville Glacier. Ellesmere Island, N.W.T., Canada. 1977; p. 28, *unpublished manuscript*.
25. Short, N.H.; Gray, A.L. Glacier dynamics in the Canadian High Arctic from RADARSAT-1 speckle tracking. *Can. J. Remote Sens.* **2005**, *31*, 225–239. [[CrossRef](#)]
26. Williamson, S.; Sharp, M.; Dowdeswell, J.; Benham, T. Iceberg calving rates from northern Ellesmere Island ice caps, Canadian Arctic 1999–2003. *J. Glaciol.* **2008**, *54*, 391–400. [[CrossRef](#)]
27. European Space Agency Science Toolbox Exploitation Platform. Available online: <https://step.esa.int/main/download/snap-download/> (accessed on 29 August 2022).
28. Nunziata, F.; Buono, A.; Migliaccio, M.; Benassai, G. Dual-polarimetric C-and X-band SAR data for coastline extraction. *IEEE J. Sel. Top. Appl. Earth Obs. Remote Sens.* **2016**, *9*, 4921–4928. [[CrossRef](#)]
29. Van Wychen, W.; Davis, J.; Burgess, D.O.; Copl, L.; Gray, L.; Sharp, M.; Mortimer, C. Characterizing interannual variability of glacier dynamics and dynamic discharge (1999–2015) for the ice masses of Ellesmere and Axel Heiberg Islands, Nunavut, Canada. *J. Geophys. Res.* **2016**, *121*, 39–63. [[CrossRef](#)]
30. Millan, R.; Mouginot, J.; Rignot, E. Mass budget of the glaciers and ice caps of the Queen Elizabeth Islands, Canada, from 1991 to 2015. *Environ. Res. Lett.* **2017**, *12*, 024016. [[CrossRef](#)]